

Design and Analysis of an 8 mW, 1 GHz Span, Passive Spectrum Scanner With >+31 dBm Out-of-Band IIP3 Using Periodically Time-Varying Circuit Components

Neha Sinha, *Student Member, IEEE*, Mansour Rachid, *Student Member, IEEE*, Shanthi Pavan, *Senior Member, IEEE*, and Sudhakar Pamarti, *Member, IEEE*

Abstract—This paper presents a low power and highly linear passive spectrum scanner based on the filtering by aliasing principle. The scanner utilizes a linear periodically time-varying circuit followed by a sampler to achieve sharp apparent filters from a continuous-time input to a discrete-time output. This paper describes the design of the scanner and provides an analysis of the expected and measured performance in the presence of circuit non-idealities. The scanner enables a DC – 1 GHz spectrum scan while consuming 8 mW of power, with an out-of-band IIP3 that is better than +31 dBm across the band.

Index Terms—Cognitive radios, discrete-time (DT) analog signal processing, IIR filters, linear periodically time varying (LPTV), RC circuits, spectrum scanner.

I. INTRODUCTION

COGNITIVE Radios [1] promise to better utilize the licensed electromagnetic spectrum by opportunistic use of any vacant frequency bands. As such, quick, accurate, spectrum sensing is a key enabling functionality. Direct digitization at the antenna, followed by filtering and energy detection in the digital domain is a desirable goal for spectrum sensing. Analog-to-digital converter (ADC) performance, however, is improving far too slowly [2] for that to be feasible in the foreseeable future. Compressive sensing-based techniques [3] can sense a sparsely populated spectrum using a much lower sampling rate than that employed by conventional techniques, thereby significantly reducing the spectrum-scan time. This technique, however, applies only to sparsely populated spectra and, when pushing to minimize the required sampling rate, requires sharp filters [4] that increase the power dissipation. In addition, they require extensive digital signal processing (DSP) in the back end, adding considerable power overhead as compared to fast Fourier transform (FFT)-based energy detection. For instance, the solution in [3] estimates the power

Manuscript received September 20, 2016; revised January 6, 2017 and March 13, 2017; accepted April 10, 2017. Date of publication May 23, 2017; date of current version July 20, 2017. This work was supported by NSF under Award ECCS 1408647. This paper was approved by Associate Editor Andrea Baschirotto. (*Corresponding author: Neha Sinha*.)

N. Sinha and S. Pamarti are with the University of California, Los Angeles, CA 90095, USA.

M. Rachid is with Silvus Technologies, Los Angeles, CA 90024 USA.

S. Pavan is with the IIT Madras, Chennai 600036, India.

Color versions of one or more of the figures in this paper are available online at <http://ieeexplore.ieee.org>.

Digital Object Identifier 10.1109/JSSC.2017.2697412

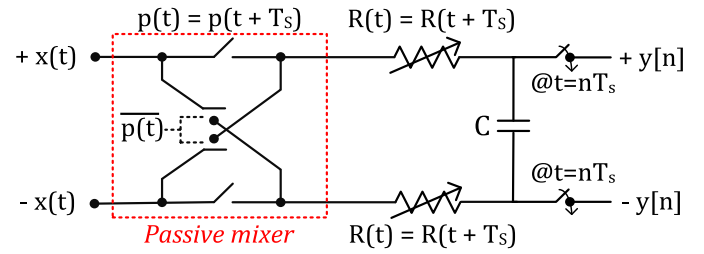


Fig. 1. LPTV RC filter.

consumption to double if the DSP processing is included. However, it should be noted that due to their significantly lower scan time requirement than traditional approaches, the work in [3] can lead to a lower energy consumption. Conventional integrated spectrum sensing techniques [5]–[8] employ a receiver-like structure. A low-noise amplifier, a down-conversion mixer, an analog low-pass anti-aliasing filter, and an ADC are typically employed to isolate and digitize a narrow spectral bin for subsequent FFT-based energy detection and thresholding [9]. The mixer's local oscillator (LO) frequency is swept to scan the spectrum. However, since the LO is typically a square wave, the conventional spectrum scanner suffers from poor harmonic rejection (HR) (i.e., suppression of signals that mix with the LOs harmonics). Moreover, since the low-pass filter (LPF) needs to be very linear and have a sharp response, it is usually realized using active components. These requirements translate into an increased power dissipation to achieve a desired dynamic range.

We recently demonstrated a spectrum scanner that resolves these problems using a passive but linear periodically time-varying (LPTV) filter circuit [10]. Our spectrum scanner achieved an out-of-band (OOB) IIP3 better than +31 dBm while dissipating 8 mW. These metrics are 21 dB and at least 4× better than prior art, respectively. At the heart of our spectrum scanner is a passive LPTV circuit shown in Fig. 1. It is a square-wave mixer followed by a simple first-order RC circuit whose capacitor voltage is sampled uniformly at a rate $F_S = 1/T_S$. The primary innovation is that the resistor R is varied periodically with a period T_S i.e., $R(t) = R(t + T_S)$. As shown later in this paper, with the square-wave mixer disabled i.e., with $p(t) = 1$, this sampled LPTV RC circuit realizes an equivalent LPF with a very sharp frequency response;

with the square-wave mixer enabled, it realizes true band-pass filters (BPF) with inherent HR. In contrast, *time-invariant* passive filters, especially those without inductors, can only achieve limited filter sharpness whereas conventional active filters consume high power and are not as linear.

We first described the central idea in signal processing terms in [11] where the technique was referred to as “Filtering by Aliasing” (FA). We demonstrated early proof of concept sharp LPTV filters in [12]. Hameed *et al.* [13] presented an active circuit version of the FA technique adopted for use directly at the antenna with additional constraints such as achieving input impedance match. As such, the circuit in [13] is significantly different and is beyond the scope of this paper. This paper is an extended version of our spectrum scanner [10]. It presents an intuitive explanation of the technique, precise design equations, and analysis of noise and other important circuit non-idealities. Note that LPTV circuits are not fundamentally new. Mixers, continuous-time delta-sigma modulators, and even the humble periodic sampler are technically LPTV circuits. This paper is different, however, in the sense that it investigates and advocates the use of time-varying circuit components. This paper is organized as follows. Section II explains the operation of and the intuition behind “how the LPTV RC circuit realizes sharp filters” from both time-domain and frequency-domain points of view. A detailed description of how the LPTV RC filter can emulate HR mixing at band-pass frequencies without active gain stages is also provided. Section III presents an accurate model that allows the design of desired filter responses and explores some design considerations. Section IV describes the design details of the passive spectrum scanner chip implemented in a 65-nm CMOS process. The effect of practical circuit non-idealities and their impacts on scanner performance are also discussed. Section V presents the measurement results of our prototype scanner. Section VI gives the conclusions.

II. OPERATION OF THE LPTV RC FILTER

For simplicity, we start by considering the low-pass version, i.e., Fig. 1 without the upfront passive mixer i.e., with $p(t) = 1$. The output of the linear time-varying system can then be written as

$$y(t) = \int_0^\infty h(t, \tau)x(t - \tau)d\tau \quad (1)$$

where $h(t, \tau)$ is the 2-D impulse response of the circuit; specifically, $h(t, \tau)$ is the response at time “ t ” for an impulse applied at time “ $t - \tau$.” For an LPTV system that varies with a period T_S , like the one in Fig. 1, $h(t, \tau)$ is periodic, i.e., $h(t, \tau) = h(t + T_S, \tau)$. The samples of the output, $y(nT_S)$, are therefore given by

$$\begin{aligned} y(nT_S) &= \int_0^\infty h(nT_S, \tau)x(nT_S - \tau)d\tau \\ &= \int_0^\infty h_{eq}(\tau)x(t - \tau)d\tau \Big|_{t=nT_S} \end{aligned} \quad (2)$$

where $h_{eq}(\tau) \stackrel{\text{def}}{=} h(nT_S, \tau) = h(0, \tau)$. In other words, sampling the output of a T_S -periodic LPTV network periodically at T_S may be thought of as sampling the output

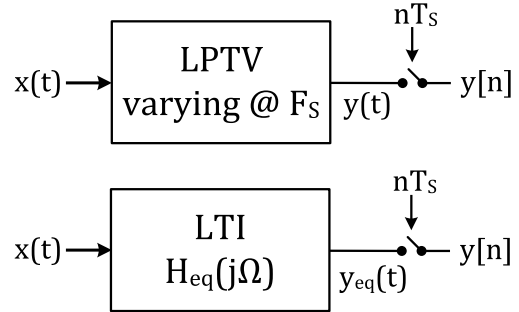


Fig. 2. Sampled LPTV system and the equivalent LTI system.

of an equivalent linear time-invariant (LTI) network with impulse response $h_{eq}(\tau)$ as shown in Fig. 2. The equivalent LTI filter impulse response $h_{eq}(\tau)$ can be derived using the “adjoint” of the circuit, as described for general sampled LPTV circuits in [14]. In our case, the circuit is simple enough that $h(t, \tau)$ and hence, $h_{eq}(\tau) = h(0, \tau)$, can be directly evaluated with ease. As shown in Appendix I

$$h_{eq}(\tau) = \frac{1}{R(-\tau)C} \exp\left(-\int_0^\tau \frac{du}{R(-u)C}\right). \quad (3)$$

Note that if $R(-\tau)$ is held constant, we get an exponentially decaying impulse response and just a simple LPF with first-order roll-off as expected. In contrast, it turns out that periodically varying R allows us to design $h_{eq}(\tau)$ in such a way that the equivalent LPF has a sharp characteristic, as shown in Fig. 3. Note from (3) that whenever $R(-\tau)$ is large (or small), $h_{eq}(\tau)$ will be accordingly small (or large). Consequently, the example sharp LPF’s impulse response can be realized by varying $R(-\tau)$, as shown in Fig. 3(b), where it can be noted that $R(-\tau)$ is large for $\tau \approx 0$ and $\tau \approx T_S$ but small at intermediate values. Thus, when compared to using a fixed resistor, a much sharper filter response is achieved. In addition, now the resistor variation can also be used to provide programmability in terms of both stopband attenuation and filter roll-off, as illustrated later.

An intriguing and insightful alternative explanation can be obtained by considering the circuit operation, again without the passive mixer, in frequency domain. First note that, essentially, a variable current, $i(t)$, is integrated onto a capacitor

$$i(t) = \frac{x(t) - y(t)}{R(t)}; \quad y(t) = \frac{1}{C} \int_{-\infty}^t i(\tau)d\tau. \quad (4)$$

The signal processing operations are depicted in Fig. 4(a), including the subsequent sampling operation. Momentarily ignore the discharging current $y(t)/R(t)$ for ease of explanation, as shown in Fig. 4(b). This assumption is reasonable at least for signals well outside the passband of the LPF. The role of $R(t)$ is now clear: it effectively serves as a variable gain, $1/R(t)$. The discharging current, $y(t)/R(t)$, is, of course, not negligible, particularly for in-band signals. Section III derives the accurate filter response and design equations including the discharging current. The central intuition described below remains valid.

The effect of the periodically time-varying resistor, $R(t)$, is to essentially “spread/mix” the input with a periodic signal,

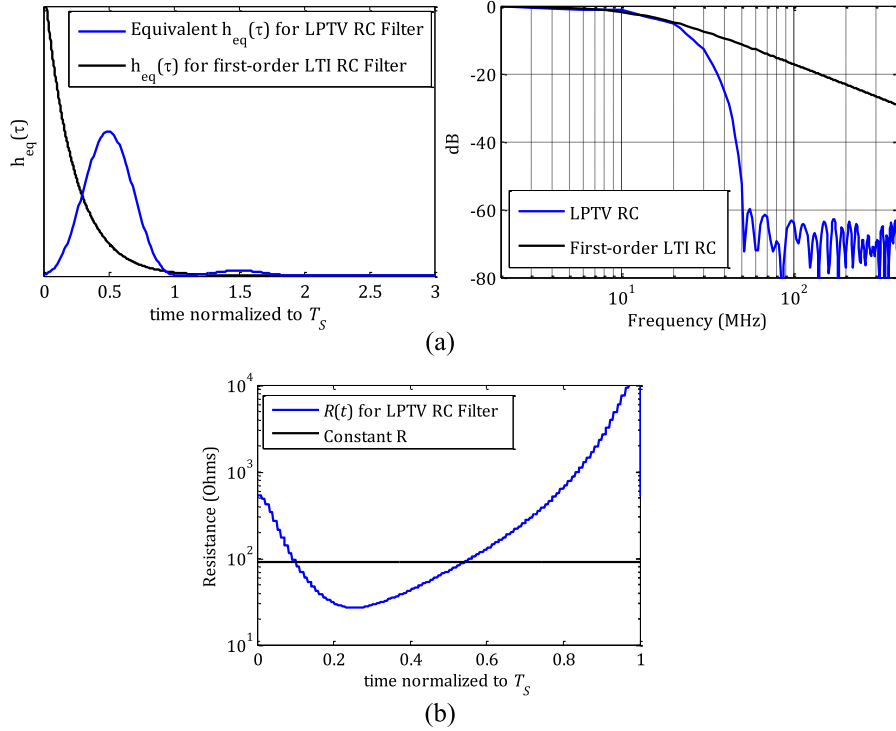


Fig. 3. (a) Example impulse response $h_{eq}(\tau)$ for a sharp LPF. (b) Resistor variation resulting in the desired $h_{eq}(\tau)$.

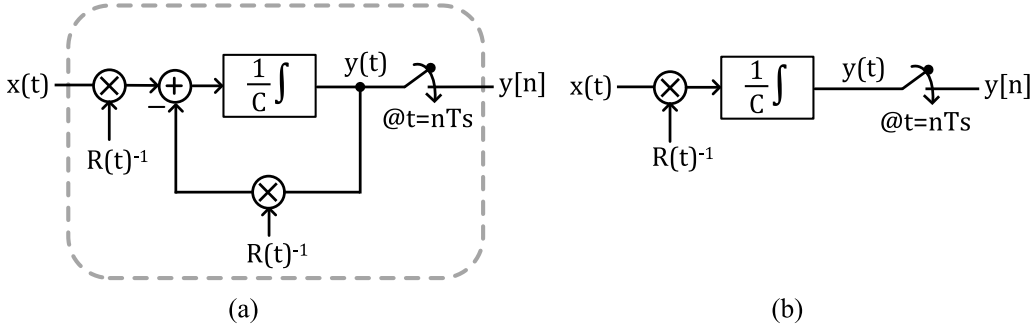


Fig. 4. (a) Equivalent signal processing operations for the LPTV RC circuit. (b) Approximate model for intuitive understanding.

$d(t) \approx 1/R(t)$, prior to filtering (integration) and subsequent sampling. Consider the frequency-domain operations illustrated in Fig. 5. Fig. 5 shows an example spectrum $X(f)$ of $x(t)$, Fourier Series coefficients D_m of the periodic $d(t)$, and the integrator response $H(f)$. As shown, spreading by $d(t)$ produces several, frequency-translated copies of the input spectrum that are weighted by D_m . These copies are further selectively weighted by the integrator. Subsequent sampling causes these various copies to alias into the $[-0.5/T_S, +0.5/T_S]$ frequency band. The various D_m [and hence $d(t)$] can be chosen such that the in-band signals are un-attenuated whereas the aliases of the OOB signals cancel each other out or are heavily suppressed. Hence the moniker, filtering by aliasing [11]. Note that the frequency selectivity of the integrator is essential to the FA concept. Without it, the subsequent aliasing would affect all the signals equally, and it would be impossible to make the copies of the in-band signal alias constructively while making those of the OOB signal alias destructively. Note also that, in a general FA system,

the integrator can be replaced by other simple, but frequency selective, filters such as first- or second-order RC filters etc.

A. LPTV RC Filter With Upfront Passive Mixer

Consider the LPTV RC filter shown in Fig. 1 again, but now with the passive mixer enabled and driven by a binary waveform $p(t)$. Assume that $p(t)$ is also periodic and has the same period as $R(t)$ so that we still have a sampled LPTV system with the sampling and repetition period T_S as before. Proceeding just like before, but using $x(t)p(t)$ instead of $x(t)$ in (1) and (2), an equivalent sampled LTI system can be readily derived with effective impulse response given by

$$g_{eq}(\tau) = \frac{p(-\tau)}{R(-\tau)C} \exp\left(-\int_0^\tau \frac{du}{R(-u)C}\right) = h_{eq}(\tau)p(-\tau). \quad (5)$$

The upfront mixer i.e., the choice of $p(t)$ allows an additional degree of freedom in the design of sharp filters.

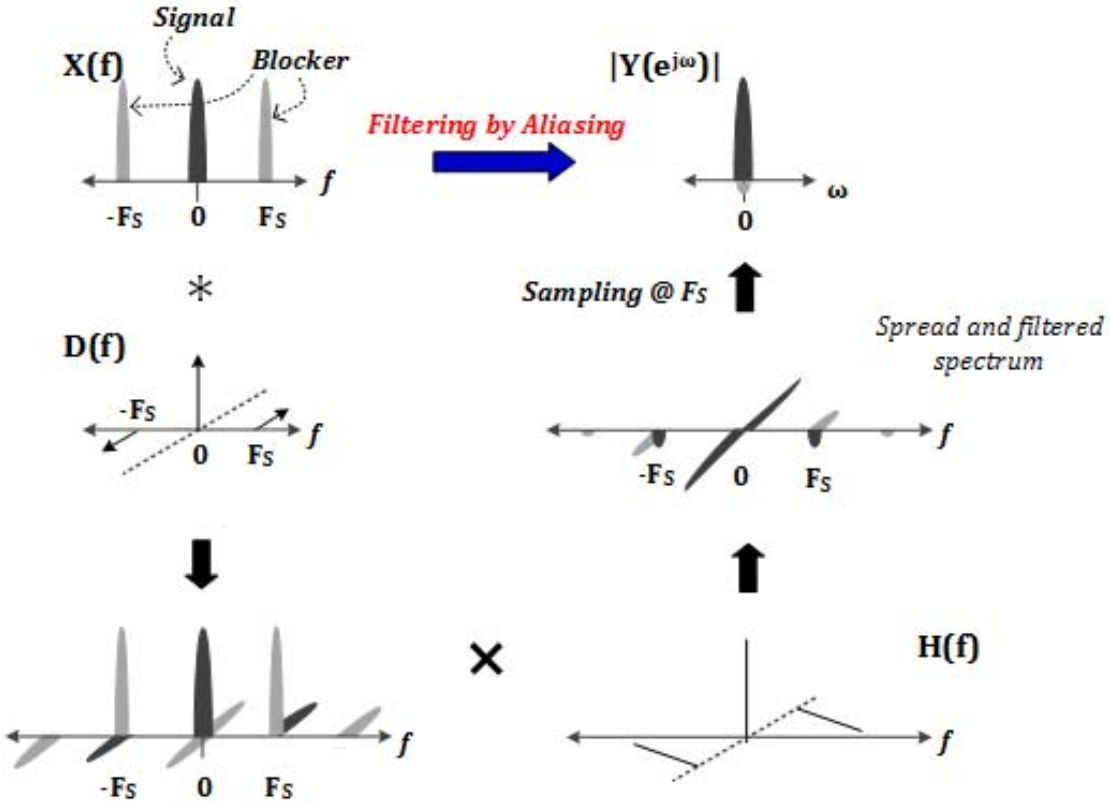


Fig. 5. Frequency-domain operations of the FA technique using an example input spectrum, $X(f)$ and spreading signal, $D(f)$. Please note that just a simple example is used here for illustration purposes.

Foremost, notice from (3) that $h_{eq}(\tau) \geq 0$. The binary (± 1) waveform $p(t)$ allows $g_{eq}(\tau)$ to be positive or negative thereby allowing even sharper filters, if required.¹ More importantly, the passive upfront mixer allows realizing very sharp BPFs using an LPTV RC LPF, as described next.

B. Band-pass Filters Without Harmonic Images

Suppose that resistor variation $R^{LP}(t)$ realizes a sharp equivalent LPF with impulse response, $h_{eq}(\tau) = h^{LP}(\tau) \geq 0$. Setting $p(t) = \text{sgn}(\cos(2\pi F_C t))$ where F_C is an integer multiple² of F_S , results in an equivalent LTI filter response, $G_{eq}(f)$, that contains copies of the sharp LPF response, $H_{eq}(f)$, translated to $f = \pm F_C$ effectively realizing sharp BPFs. This makes intuitive sense owing to the similarity with mixer-first approach. However, since $p(t)$ also contains the harmonics of F_C , such square-wave mixing results in undesired band-pass images at the harmonics, just like in conventional mixer-first approach.

Interestingly, these harmonic images can be eliminated in the LPTV RC filtering technique using a simple trick. What is desired is true sinusoidal multiplication of the input, $x(t)$. Since the square-wave mixer only multiplies by the “sign” of the sinusoid, $p(t) = \text{sgn}(\cos(2\pi F_C t))$, we appropriately

¹There may be an attendant in-band signal loss, and for the sake of simplicity, this option is not considered anymore in this paper.

² F_C does not have to be an integer multiple of F_S for band-pass operation. However, it is assumed to enable harmonic rejection as described.

weigh the input according to the envelope of the sinusoid using the variable $R(t)$. Specifically, we choose a new resistor variation, $R(t)$, such that $h_{eq}(\tau) = |\cos(-2\pi F_C \tau)|h^{LP}(\tau)$. It follows that the impulse response of the equivalent LTI filter is $g_{eq}(\tau) = h_{eq}(\tau)p(-\tau) = \cos(-2\pi F_C \tau)h^{LP}(\tau)$. Consequently, $G_{eq}(f) = 0.5 \cdot [H^{LP}(f - F_C) + H^{LP}(f + F_C)]$, a true band-pass filter without harmonic images. Fig. 6 illustrates the effective BPF with harmonic suppression.

III. DESIGN OF LPTV RC FILTER

Previous sections, especially (3), do not readily suggest how to quantitatively choose $R(t)$ so as to achieve a desired impulse response $h_{eq}(\tau)$. Towards this purpose, we restrict our attention to the practical case where $R(t)$ and $p(t)$ are varied in time-steps³ of T_{CLK} where $T_{CLK} \ll T_S$. Accordingly, suppose that R_η is the repeating sequence of resistor values with period $K = T_S/T_{CLK}$ that determines the periodic resistor variation $R(t)$ i.e., $R_\eta = R(\eta T_{CLK})$ where $\eta = 0, 1, 2, \dots$. Similarly p_η represents the binary mixer control waveform.⁴ For instance, for a BPF at F_C , $p_\eta = \text{sgn}(\cos(2\pi F_C \eta T_{CLK}))$ where F_C is

³It is possible to realize $R(t)$ as a continuously varying resistor, perhaps using a transistor in triode region of operation. However, from a linearity point of view, it may be easier and preferable to vary it in a discrete manner, using a switchable bank of resistors as described in Section IV.

⁴While not necessary, we discretize the mixer switching waveform, $p(t)$, at the same rate as (and in sync with) the resistor variation, $R(t)$. This avoids synchronization errors between $p(t)$ and $R(t)$, which may otherwise degrade filter performance including harmonic rejection.

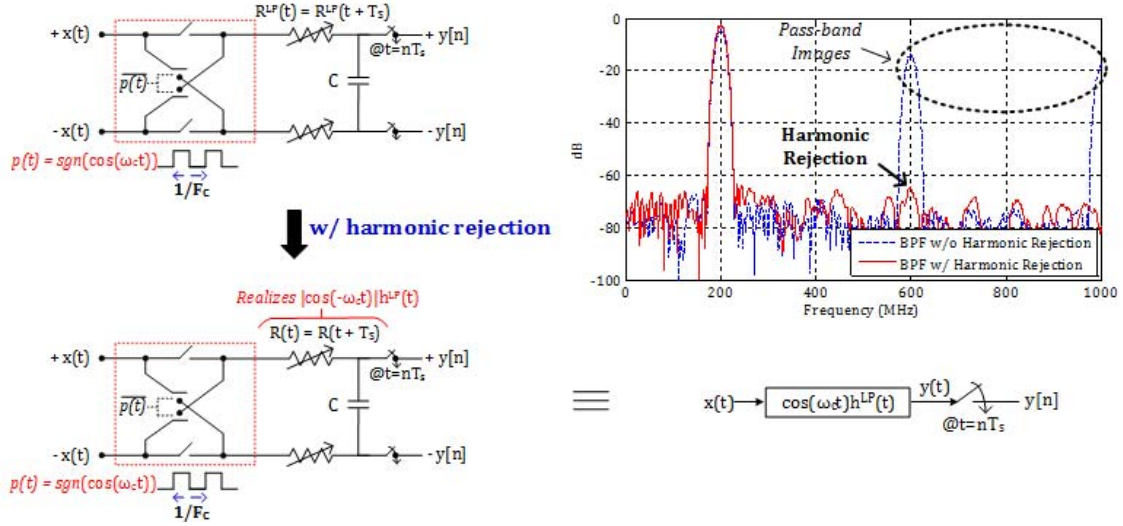


Fig. 6. BPF with sine-wave mixing for HR using the LPTV RC filter, and its equivalent model.

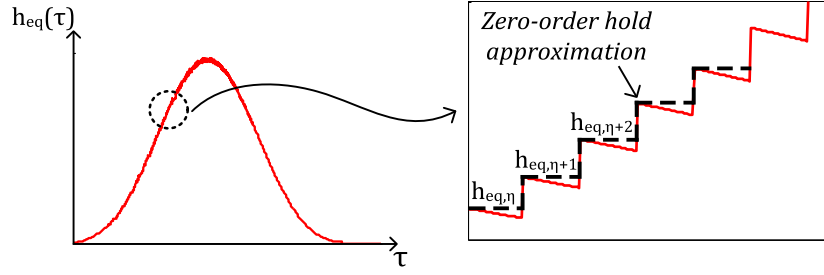


Fig. 7. Example $h_{eq}(\tau)$ waveform showing the zero-order hold approximation.

an integer multiple of F_S . Below, we derive an expression for the equivalent filter response, $G_{eq}(f)$, in terms of R_η and p_η .

Since both $R(t)$ and $p(t)$ are varied in steps of T_{CLK} , it follows from (3) that both $h_{eq}(\tau)$ and $g_{eq}(\tau)$ can be closely approximated by a zero-order hold interpolation of their respective samples, $h_{eq,\eta} \stackrel{\text{def}}{=} T_{CLK}h_{eq}(\eta T_{CLK})$ and $g_{eq,\eta} \stackrel{\text{def}}{=} T_{CLK}g_{eq}(\eta T_{CLK}) = p_\eta h_{eq,\eta}$. For example

$$g_{eq}(\tau) \approx \sum_{\eta=0}^{\infty} p_\eta h_{eq,\eta} g_0(\tau - \eta T_{CLK})$$

$$\text{where } g_0(\tau) = \begin{cases} 1/T_{CLK}, & 0 \leq \tau < T_{CLK} \\ 0, & \text{else.} \end{cases} \quad (6)$$

Fig. 7 illustrates this using an example low-pass $h_{eq}(\tau)$ variation. From (3), the samples $h_{eq,\eta}$ can be readily shown to be

$$h_{eq,\eta} = \frac{T_{CLK}}{R_{-\eta} C} e^{-\sum_{k=0}^{\eta-1} \alpha_k} = \alpha_\eta \prod_{k=0}^{\eta-1} e^{-\alpha_k} \approx \alpha_\eta \prod_{k=0}^{\eta-1} (1 - \alpha_k) \quad \forall \eta = 0, 1, 2, \dots \quad (7)$$

where $\alpha_k = T_{CLK}/R_{-\eta} C$ and $R_{-\eta} = R_{K-\eta}$ as it is periodic. Here, we have assumed that $T_{CLK} \ll R_{-k} C$. While technically not required, this would be the most likely scenario. From

the periodicity of R , it follows that $h_{eq,\eta+K} = \beta h_{eq,\eta}$, where $\beta = \prod_{\eta=0}^{K-1} (1 - \alpha_\eta)$. It can be shown that the sequence of samples, $g_{eq,\eta}$, represent a discrete-time IIR filter with frequency response

$$G_{eq}(e^{j\omega}) \stackrel{\text{def}}{=} \sum_{\eta=0}^{\infty} g_{eq,\eta} e^{-j\omega\eta} = \sum_{\eta=0}^{\infty} p_\eta h_{eq,\eta} e^{-j\omega\eta} \cong \frac{\sum_{\eta=0}^{K-1} (p_\eta \alpha_\eta) \left(\prod_{i=0}^{\eta-1} (1 - \alpha_i) \right) e^{-j\omega\eta}}{1 - \left(\prod_{\eta=0}^{K-1} (1 - \alpha_\eta) \right) e^{-j\omega K}}. \quad (8)$$

Now, using (6), the LPTV RC system has an equivalent LTI filter frequency response given by

$$G_{eq}(j\Omega) \approx G_{eq}(e^{j\Omega T_{CLK}}) \cdot \text{sinc}\left(\frac{\Omega T_{CLK}}{2}\right). \quad (9)$$

The LPTV RC filter can therefore be equivalently represented by the model shown in Fig. 8. Fig. 8 also shows the relationship between R_η , p_η and the impulse response of the equivalent filter $g_{eq,\eta}$. Filter design can now proceed using traditional means by determining R_η and p_η needed to realize desired $G_{eq}(e^{j\omega})$ and hence, $G_{eq}(j\Omega)$.

Two things are of note. First, the denominator of $G_{eq}(e^{j\omega})$ represents K poles that are equidistant from the origin and evenly distributed from 0 to 2π in the z -plane, creating an

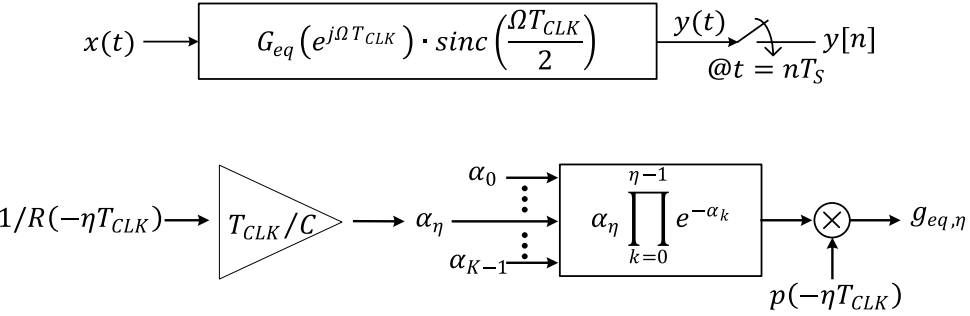


Fig. 8. (Top) Equivalent frequency response of the LPTV RC filter. (Bottom) Signal processing operations needed to obtain the η^{th} sample ($\eta = 0, 1, \dots$) of the impulse response of $G_{eq}(e^{j\omega})$, where $R(t) = R(t + T_S)$ and $p(t) = p(t + T_S)$ are the periodic resistor variation and mixer control signals, respectively.

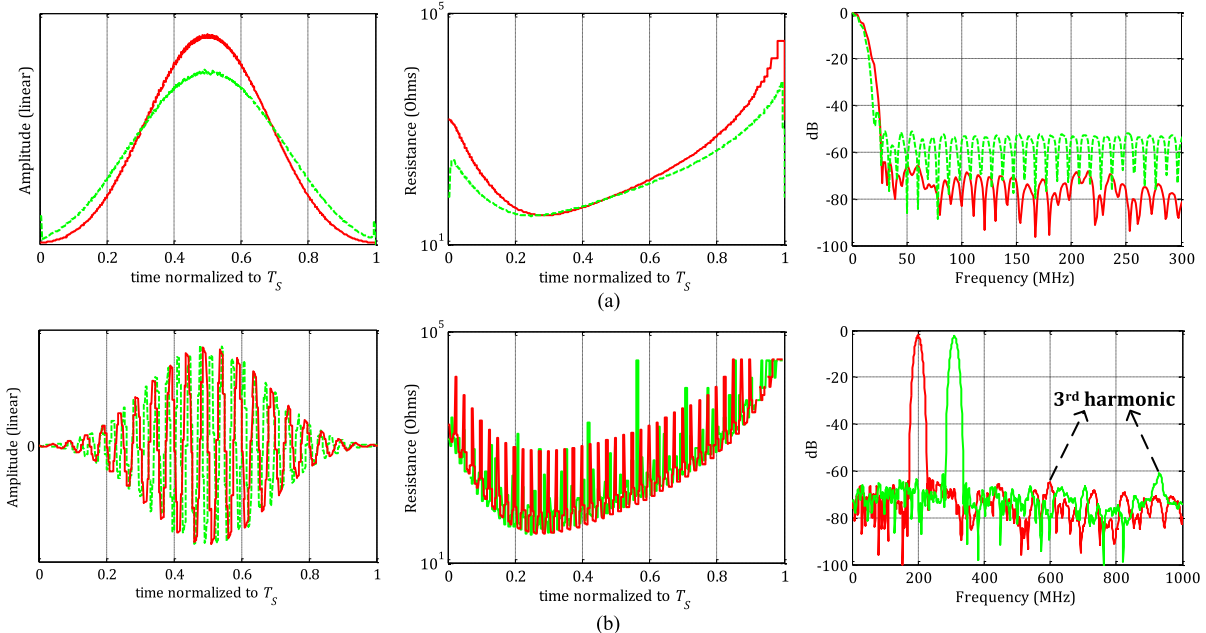


Fig. 9. (a) (Left to right) Impulse responses for two example LPF, corresponding $R(t)$ variations and their frequency responses. (b) (Left to right) Impulse response for two example BPF at 200 and 310 MHz, corresponding $R(t)$ variations and their frequency responses with HR.

approximate all-pass response for reasonably large K . So, the denominator's effect on the filter suppression or sharpness is not critical. Second, a BPF with HR can be realized by setting

$$\begin{aligned} p_\eta &= \text{sgn}(\cos(2\pi F_C \eta T_{CLK})) \text{ and} \\ h_{eq,\eta} &= h_{eq,\eta}^{\text{LP}} \cdot |\cos(-2\pi F_C \eta T_{CLK})| \end{aligned} \quad (10)$$

where $h_{eq,\eta}^{\text{LP}}$ is the impulse response of an LPF. A detailed design procedure is presented after a discussion of practical considerations in the implementation of the LPTV filter.

Fig. 9 shows an example low-pass and with their impulse responses and the corresponding resistor variations and filter responses. It can be seen how the resistor variation for HR differs from its low-pass counterpart. Now for each center frequency, a new resistor (and mixer) waveform can be used to scan different frequency bins in a given frequency span.

Note that the equivalent LTI filter transfer function can be obtained by other means as well. For instance, as we originally suggested in [11], the integro-differential equations that govern the LPTV RC circuit could be directly discretized using an

appropriate integration formula. An alternative, and perhaps more intuitive (to the circuit designer) approach involves a direct time-domain analysis of the simple first-order RC circuit during each time-step, T_{CLK} . Assuming that the input is constant during this small time-step, it is easy to show that

$$\begin{aligned} y(\eta T_{CLK}) &= p_\eta \cdot x(\eta T_{CLK})(1 - e^{-\alpha_\eta}) \\ &\quad + y(\eta T_{CLK} - T_{CLK})e^{-\alpha_\eta} \end{aligned} \quad (11)$$

where $y(t)$ is the voltage on the capacitor and the two terms in the right-hand side correspond to the simultaneous charging and discharging of the capacitor during the η^{th} T_{CLK} time-step. Similar expressions for $G_{eq}(e^{j\omega})$ can be obtained by repeated application of this equation over successive time-steps.

A. Practical Considerations

Since the LPTV resistance $R(t)$ is assumed to be varied only at a finite rate, $F_{CLK} = 1/T_{CLK}$, it will cause filter images

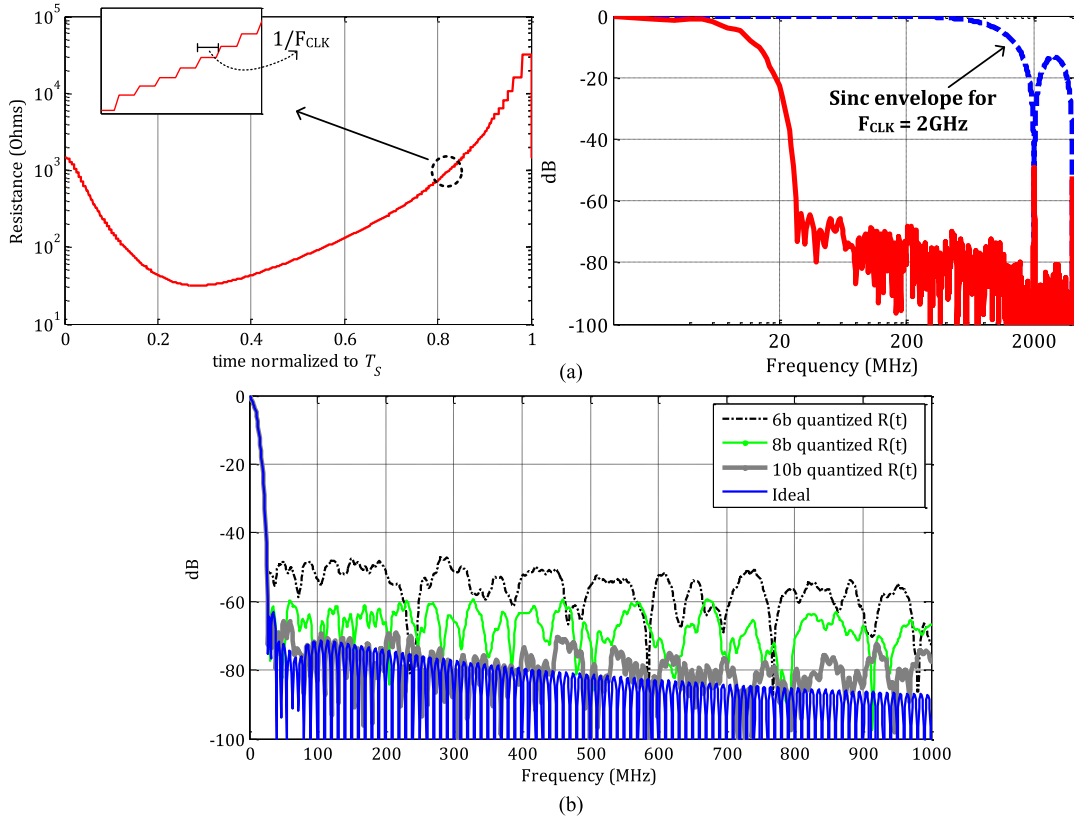


Fig. 10. (a) Finite rate of resistor variation resulting in *sinc* shape. (b) Effect of resistor quantization on filter response.

to appear at integer multiples of this frequency, as shown in Fig. 10(a). This is also evident from (9) where $G_{eq}(e^{j\Omega T_{CLK}})$ is periodic. Ideally, the switching frequency F_{CLK} should be as high as possible but practical considerations such as power consumption, and technology node limit how high it can be. The images, however, are attenuated by the *sinc* filtering (9). It should be noted that since the capacitor voltage is the result of an *RC* operation and not a perfect sampled-and-held signal, the images at multiples of F_{CLK} are not perfectly nulled. They are, however, greatly suppressed. For instance, as shown in Fig. 10(a), the first image is nulled by ~ 50 dB. Practical implementations will also inevitably result in less-than-abrupt jumps in $R(t)$ resulting in additional filtering of the switching images, just as in any digital-to-analog converter. Note also that the resistance values can only be varied in finite steps, meaning that they need to be quantized. Fig. 10(b) shows the effect of resistor quantization on the filter response. As can be seen, 10-bit resistor quantization is sufficient to achieve ~ 70 dB stopband attenuation together with a transition bandwidth that is $4\times$ the filter BW.

The mean square noise voltage across the capacitor of the LPTV *RC* filter, and hence, in its output samples is kT/C , just as in an LTI *RC* filter. Appendix II mathematically proves this, and measurements of the prototype IC described later in this paper confirm it. As an example, consider a sharp LPTV *RC* filter with a -3 dB bandwidth of 7 MHz. With $R(t)$ variation chosen such that $\min(R(t) + R_S) = 30\Omega$, a capacitor value $C = 470$ pF gives the desired sharp filter

shown in Fig. 11 and results in an output noise of $3 \mu\text{V}_{\text{rms}}$. In comparison, a first-order *RC* filter needs $C = 910$ pF with a constant resistance of 25Ω to give a filter with the same -3 dB bandwidth. This has lower noise, but only a 20-dB/dec roll-off. A second order *RC*-*RC* filter can achieve close to 40-dB/dec roll-off (as shown in Fig. 11), but needs much lower output capacitance, C_2 which leads to a higher noise. Compared to this, the LPTV *RC* filter has better sharpness, lower noise, and less total capacitance. A thorough discussion of the benefits offered by LPTV filters in the context of filter sharpness versus noise tradeoff, compared to other passive filters, is the subject of another paper. It is also worthwhile to note that the scanner presents high impedance at its input. It is a time-varying resistance in series with a capacitor with the mean($R(t)$) $\gg 50 \Omega$. This results in the S_{11} being high as confirmed by the measurements shown in Section V.

B. Design Procedure

We now illustrate the design procedure using an example filter design. To enable the scan of a 1 GHz spectrum with a 10 MHz RBW, we start by choosing $F_{CLK} = 2$ GHz and design a LPF with bandwidth, $BW = 5$ MHz. F_{CLK} is chosen to be 2 GHz since filter images appear at this frequency, as mentioned in Section III-A. The LPF bandwidth is chosen to be half the desired RBW. The output sampling rate, F_S for these filters is chosen to be $2 \cdot BW$. Assume that C is chosen

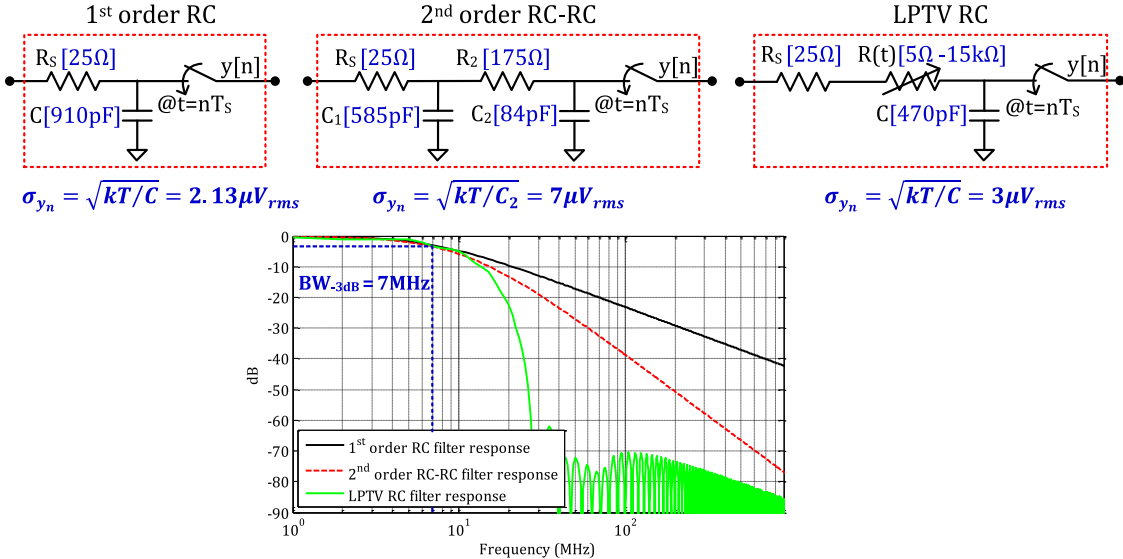


Fig. 11. Comparison of noise-sharpness tradeoff between passive LPTV and LTI RC filters.

large enough to render the sampled output noise variance, kT/C , small enough. Assume that the source has a differential source resistance R_S . This can be included in the design as $R(t) \stackrel{\text{def}}{=} R_S + R'(t)$, where $R(t) = R(t + T_S)$ is the total periodically varying resistance.

- 1) Design K^{th} -order FIR LPF $h_{\text{eq},\eta}^{\text{LP}} \geq 0$, with bandwidth, BW, where $K = F_{\text{CLK}}/F_S$; e.g., $K = 200$.
- 2) Set $p_\eta = \text{sgn}(\cos(2\pi F_C \eta T_{\text{CLK}}))$ and $h_{\text{eq},\eta} = h_{\text{eq},\eta}^{\text{LP}} \cdot |\cos(-2\pi F_C \eta T_{\text{CLK}})|$ where F_C is the desired center frequency for the BPF.
- 3) Use (7) to compute α_η recursively from $\eta = 0$. It can be shown that $\alpha_\eta = h_\eta \prod_{k=0}^{\eta-1} e^{\alpha_k}$.
- 4) Calculate the resultant R_η , given α_η . If $\min(R_\eta) \leq R_S$, it is not realizable. So, reduce C and repeat this step, or go to Step 1 and design a relaxed filter.
- 5) Quantize to chosen number of bits.

Note that the minimum possible R_η imposes a tradeoff between the minimum noise and achievable stopband attenuation for a given number of bits. Hence, a few iterations may be required to achieve target performance. Note also that once a resistor digital-to-analog converter (DAC) (RDAC) has been chosen (i.e., number of bits, minimum R_η), the capacitance C needs to be varied with varying bandwidths.

In this paper, convex optimization [15] and spectral factorization [16] are used to find the optimal squared magnitude $|H_{\text{eq}}^{\text{LP}}(e^{j\omega})|^2$, and the corresponding minimum phase $H_{\text{eq}}^{\text{LP}}(e^{j\omega})$ and $h_{\text{eq},\eta}^{\text{LP}}$. The same LPF is used for all the bins while F_C is swept and accordingly new $h_{\text{eq},\eta}$, R_η , and p_η are calculated. Note that for BPF with HR, $h_{\text{eq},\eta}$ can become very small for some F_C . Correspondingly, R_η can be very large. However, a 10-bit $R(t)$ variation is sufficient to get good HR.

IV. CHIP IMPLEMENTATION

Fig. 12 shows the block diagram of the designed IC which was implemented in TSMC 1P6M 65-nm CMOS process.

The main components of the chip are a resistor DAC with an integrated mixer, capacitor banks, clock generation circuitry, and digital control blocks.

A. Resistor DAC With Integrated Mixer

A straightforward implementation of an RDAC with a passive mixer is shown in Fig. 13(a) and was realized in [12]. This simple structure suffers from two drawbacks: 1) the upfront mixer switches are subjected to the entire input signal swing which degrades filter linearity and 2) the high parasitic capacitance associated with the mixer switches leads to unwanted charge loss paths that degrade both stopband attenuation and HR. The second effect is a result of the mixer switches being sized up so as to not limit the minimum achievable resistance in $R(t)$.

A better RDAC structure with an integrated mixer, shown in Fig. 13(b), resolves both issues. This RDAC is implemented differentially and consists of two nominally matched 10-bit resistor ladders. The RDACs consist of binary-weighted *rppoly* resistors in series with transmission gate switches. The switch in each branch is scaled with the resistance in the branch: smaller switches in series with larger resistors. The RDAC is designed to have a minimum resistance of 33Ω with the switch in each branch sized to have an ON-resistance that is 10% of the poly resistance.

The desired resistor variation, $R(t)$ and mixer control, $p(t)$ is obtained by driving the RDAC switches using the 10-bit resistor control, $R_{\text{cont}}(9:0)$ and 1-bit mixer control, Mix_{cont} , respectively, from the digital block. These controls are generated at F_{CLK} that is nominally set at 2 GHz to scan a 1 GHz frequency span. The switch in each branch of this new RDAC is controlled by a logical AND between the mixer control, Mix_{cont} and the resistor control $R_{\text{cont}}(9:0)$. This way, depending on the mixer control, either a *through-* or *cross-*branch of the RDAC is activated. For example, a filter at $F_C = F_{\text{CLK}}/2$ has $\text{Mix}_{\text{cont}} = \dots +1, -1, +1, -1, \dots$, turning

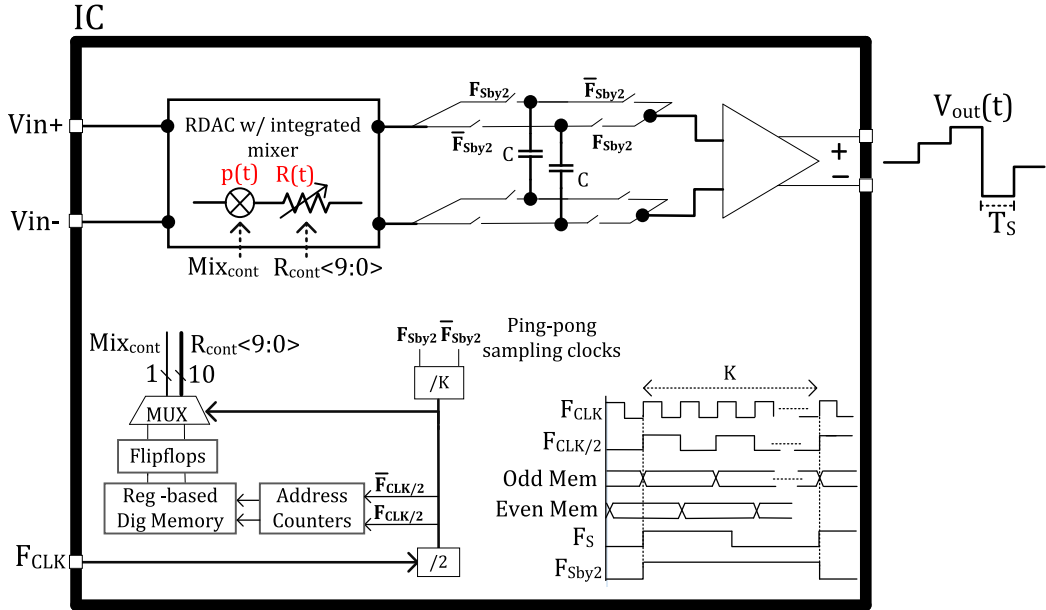


Fig. 12. Block diagram of fabricated spectrum scanner IC.

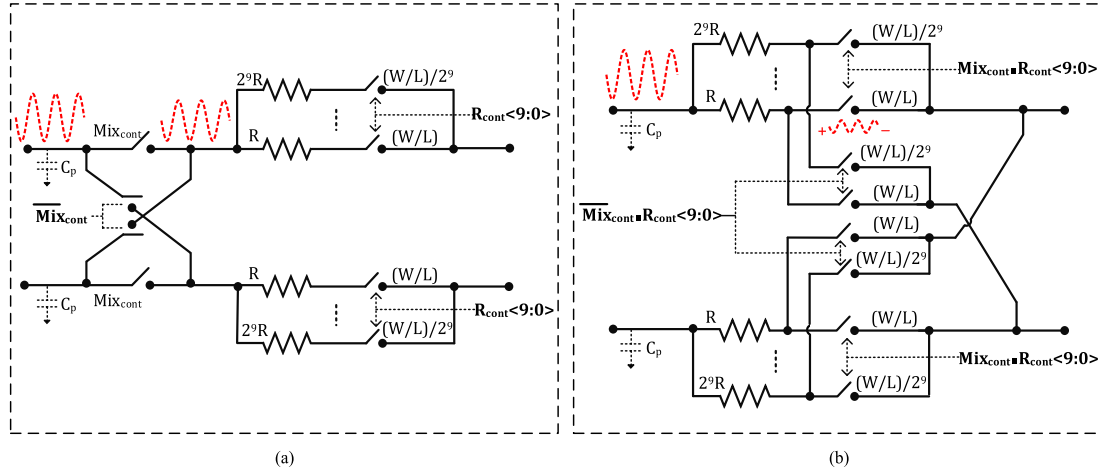


Fig. 13. (a) Naïve RDAC and mixer implementation [12]. (b) Superior RDAC with integrated mixer offering better linearity.

ON the *through-* and *cross*-branches of the RDAC alternatively. A 1.2 V supply drives these controls to maximize linearity with the provided DC bias of 0.6 V.

1) Circuit Parasitics: Fig. 14 shows the single-ended RDAC circuit modified to explicitly show the switch and wire parasitics. The parasitics modify the equivalent LTI filter impulse response $g_{eq}(t)$, thereby degrading the filter response.

a) Parasitic Capacitance C_{ds} : In the naïve RDAC implementation [12], the achievable stopband attenuation is significantly limited by the C_{ds} capacitance of the transmission gate switches. Since the $R - C_{ds}$ cutoff frequency in the OFF-branches is significantly higher than the frequencies of interest, the RDAC structure in [12] can be reduced to the one shown in Fig. 15(a), where the C_{ds} of the OFF-portion provides a conductive path that could bypass the ON-portion, especially for small values of n .

In the proposed RDAC with an integrated mixer, the effect of C_{ds} is reduced, as shown in Fig. 15(b). With the mixer

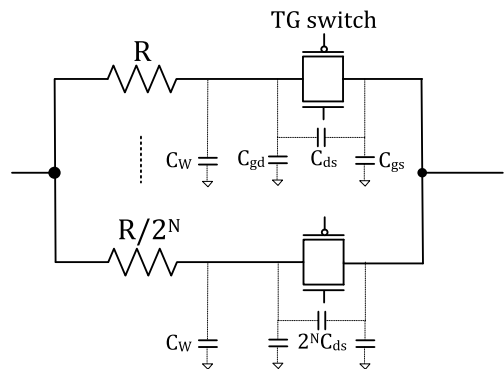


Fig. 14. Single-ended RDAC structure with parasitics.

incorporated in the RDAC switches, based on the resistor control code n and the mixer control, either some of the *through*-branches and all the *cross*-branches of the RDAC are OFF or vice-versa. Then, as illustrated with the example in

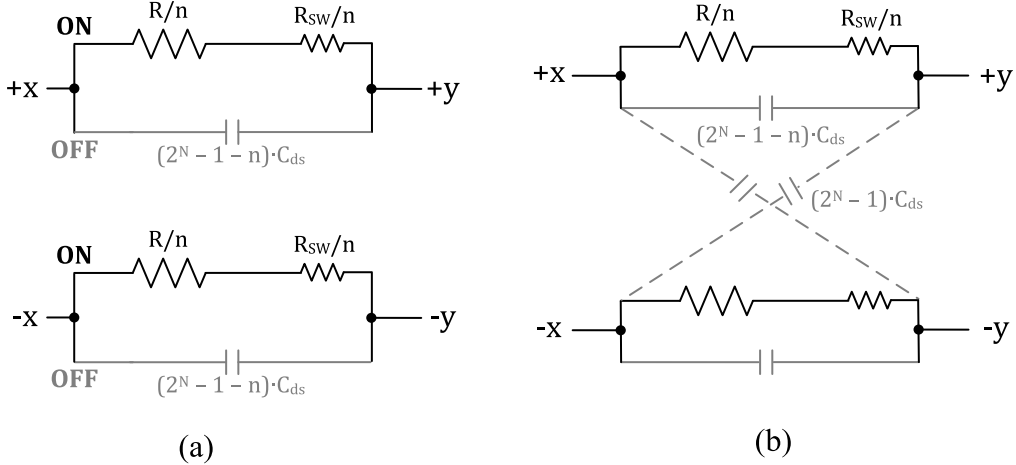


Fig. 15. (a) Equivalent differential structure with C_{ds} capacitance for the naïve implementation of the RDAC [12]. (b) Equivalent schematic showing C_{ds} capacitance for the improved RDAC with integrated mixer.

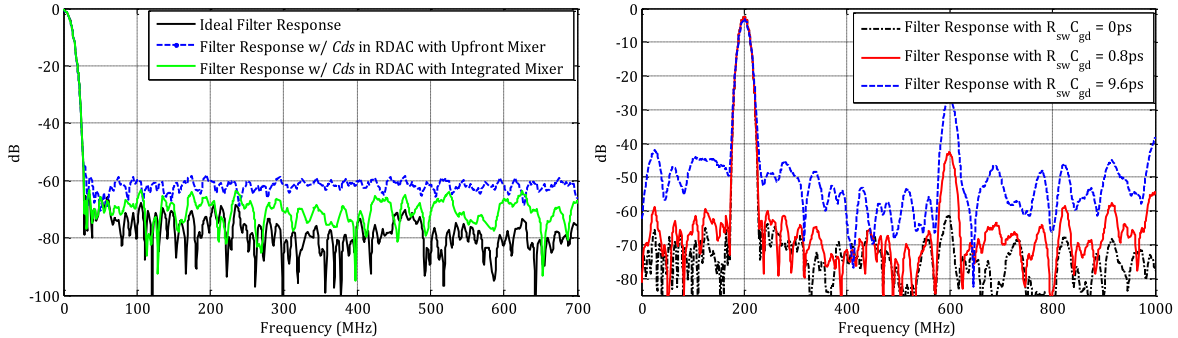


Fig. 16. Simulated effect of switch parasitics on filter suppression and HR.

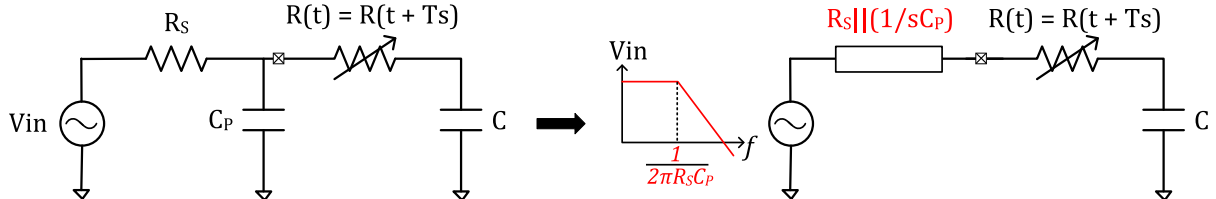


Fig. 17. Equivalent circuit in the presence of source resistance R_S and input capacitance C_P .

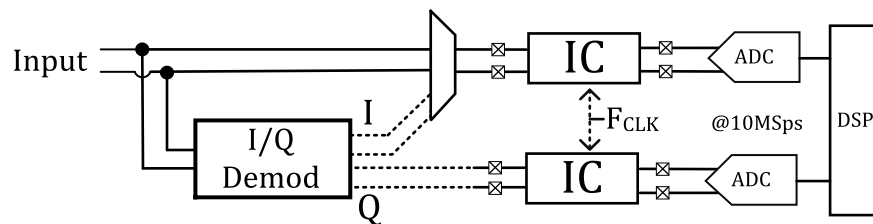


Fig. 18. System setup for testing.

Fig. 15(b), the presence of additional C_{ds} capacitances in the OFF cross-path help cancel some of the parasitic currents in the through-path. Now for smaller values of n , most of the parasitic currents cancel out. However, for large values of n , the net parasitic capacitance increases, but its parallel resistance decreases (unlike the structure in Fig. 15(a)), and

hence, the error introduced in the output voltage is reduced. As shown in Fig. 16, this helps reduce the impact of C_{ds} on the filter response. Note, however, that C_{ds} is not canceled completely and hence there is still some worsening of the stopband attenuation. When realizing BPF, the change in the filter coefficients due to C_{ds} also causes distortion in the

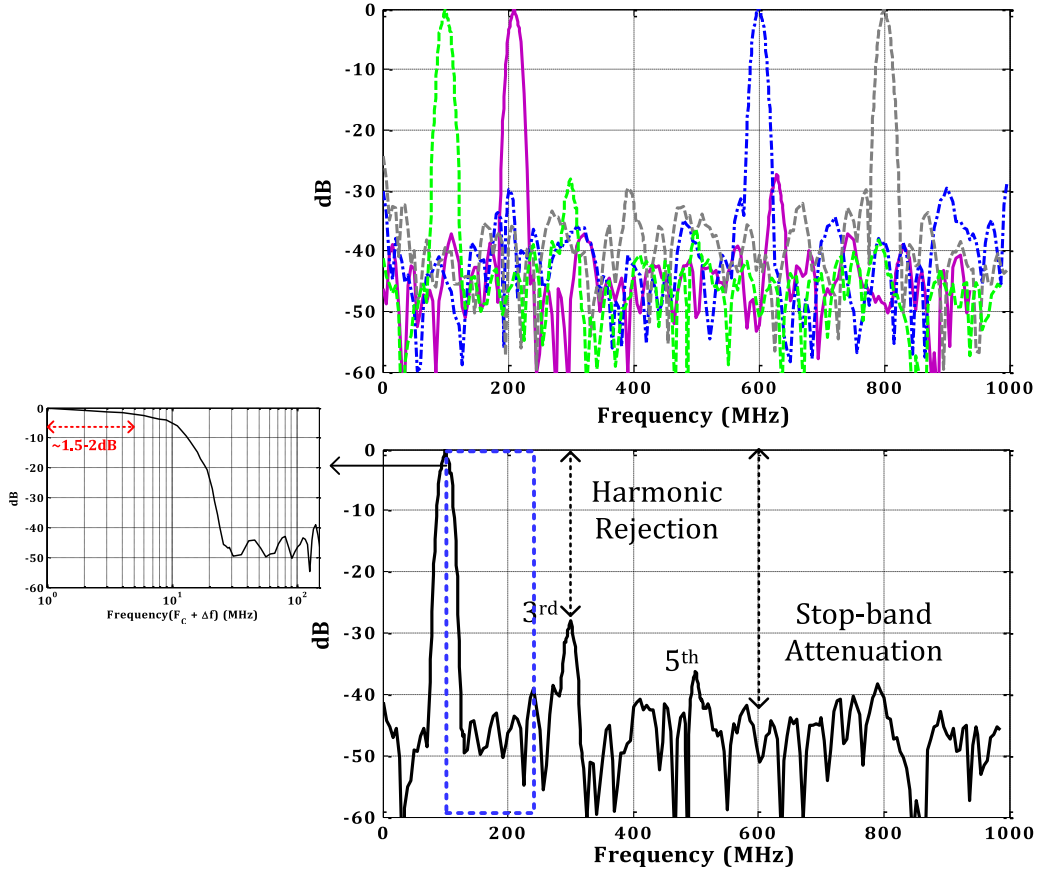


Fig. 19. (Top) Measured 10 MHz filters at different center frequencies (normalized). (Bottom) Representative measured filter at 100 MHz showing the harmonic response and stopband attenuation.

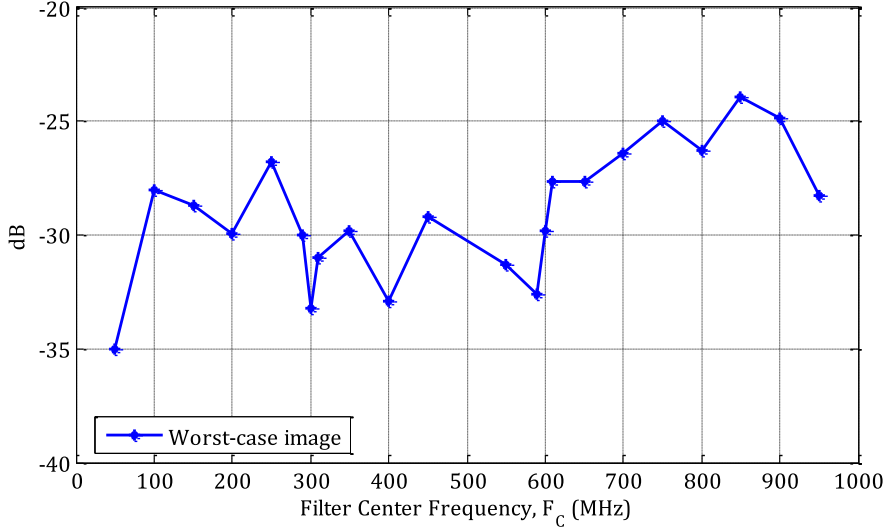


Fig. 20. Worst case spurious image versus filter center frequency F_C .

envelope of the sinusoid, and hence adversely affects HR as well.

b) Parasitic Capacitance C_{gs} , C_W , and C_{gd} : The C_{gs} capacitance shown in Fig. 14 is always present in parallel with a much larger (~ 2 to 3 orders of magnitude) capacitor C and hence does not have an impact on the filter response. C_{gd} and C_W (wire) capacitances, on the other hand, manifest themselves in a rather complicated manner. Based on the

resistor branches that turn ON from one instance to the next, variable amount of parasitic C_{gd} and C_W capacitances share charge with the load capacitor C . This time-varying charge sharing alters the output voltage on the capacitor from its nominal value leading to degraded stopband attenuation and HR.

HR relies on perfect sinusoidal mixing through the accurate realization and timing of the resistor value changes and the

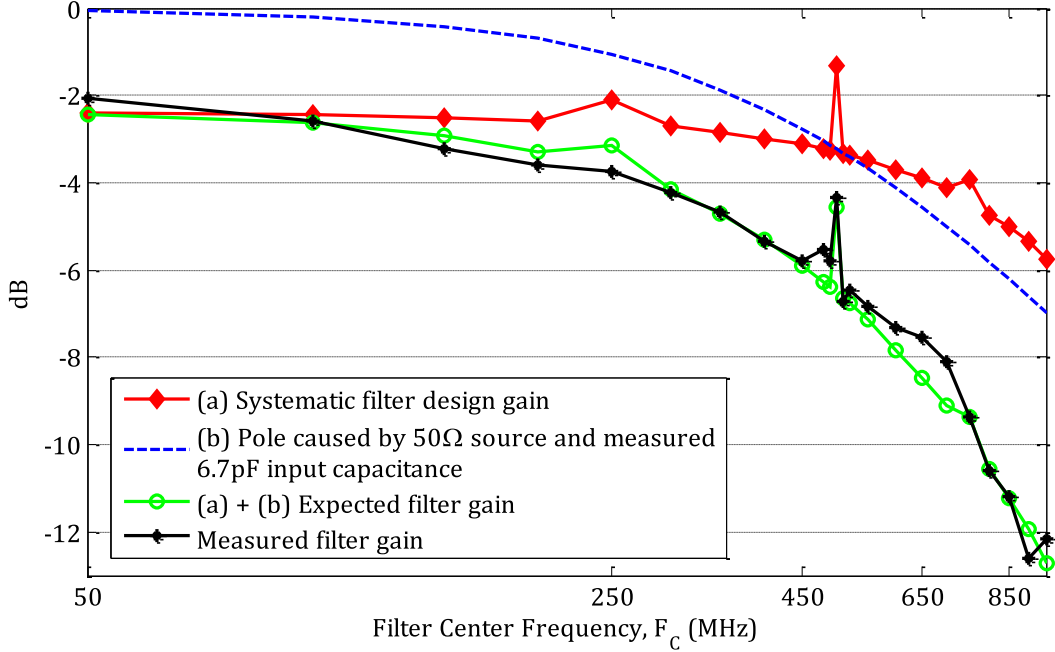


Fig. 21. Gain versus filter center frequency F_C .

sign-switching events. This leads to HR being much more sensitive to the presence of parasitic capacitances in the RDAC. The simulated effect of the C_{gd} (and C_W) parasitic capacitances from the RDAC on HR and stopband attenuation of the filters is shown in Fig. 16.

c) *Input Capacitance C_P :* The effects of the input parasitic capacitance C_P are best understood using the equivalent circuit shown in Fig. 17, obtained using source transformations. First, the input voltage source is low-pass filtered which lowers the in-band gain of BPFs with high center frequencies, as demonstrated in Section V. Second, the HR is further degraded as it relies on a perfect input source with constant resistance to achieve accurate sinusoidal envelope tracking. Another intuitive perspective is that the upfront LPF formed by the frequency dependent input source impedance affects the relative gain of the harmonic images being rejected by the FA circuit.

2) *Circuit Non-Linearity:* The non-linearity of the filter is dominated by the switches used for the RDAC, more specifically by their non-linear resistance and capacitance. The use of transmission gates with a DC bias that is half the supply voltage, helps mitigate some of the non-linearity. As mentioned previously, the removal of explicit upfront mixer switches helps improve the linearity by ~ 9 dB compared to our work in [12]. This is because, as shown in Fig. 13(b), the presence of series poly-resistors with resistance that is $10\times$ the ON-resistance of the switches helps shield the RDAC switches from the large input signal swings.

B. Capacitor Banks

The RDAC is followed by ping-pong output capacitor banks, C , allowing one capacitor's output to be read while the other is used in the filter. As noted in Section III, since the resulting IIR poles of the apparent filter response

[denominator of $G_{eq}(e^{j\omega})$ in (8)] have minimal effect on the filter suppression, the ping-pong operation is used for ease of circuit implementation and chosen to demonstrate successful FA using simple sampling elements. The capacitor banks can be statically programmed to allow additional filter programmability. They are 5-bit binary-controlled MIM capacitors and have a tuning range from 6.5 to 201.5 pF. The parasitics associated with the static control switches of the capacitor banks have no effect on the filter response.

C. Digital Control Unit and Clock Generation

The resistor sequence bits, $R_{\text{cont}}(9:0)$, and the mixer-switching bit, Mix_{cont} , are periodic with $K = F_{\text{CLK}}/F_S$ and stored in register-based memory. They are generated offline using MATLAB for the desired frequency bin and loaded on chip. Since the sequence is read at the input rate ($F_{\text{CLK}} = K F_S$), the memory is split into equal halves corresponding to odd and even periods of F_{CLK} . A half-input-rate clock $F_{\text{CLK}/2}$, repeats a counter (counting from 1 to $K/2$) to provide addresses to sequentially read these memory registers. A 2:1 MUX running on $F_{\text{CLK}/2}$ toggles between the odd and even halves. This arrangement is chosen to allow for the high input rate operation with a minimal power cost. The 11 bits are then buffered to control the switches in the RDAC. The output sampling clock, F_S , is generated by dividing F_{CLK} by K . Since the bandwidth of the designed filters is $F_S/2$, bandwidth programmability is enabled by changing the division ratio K . F_{CLK} is itself generated from an off-chip differential clock signal buffered on chip. The digital and clock generation circuitry run on a 1 V supply.

V. MEASUREMENT RESULTS

The chip measurements were made using two setups, as shown in Fig. 18: 1) Using a $50\ \Omega$ source that is directly AC-

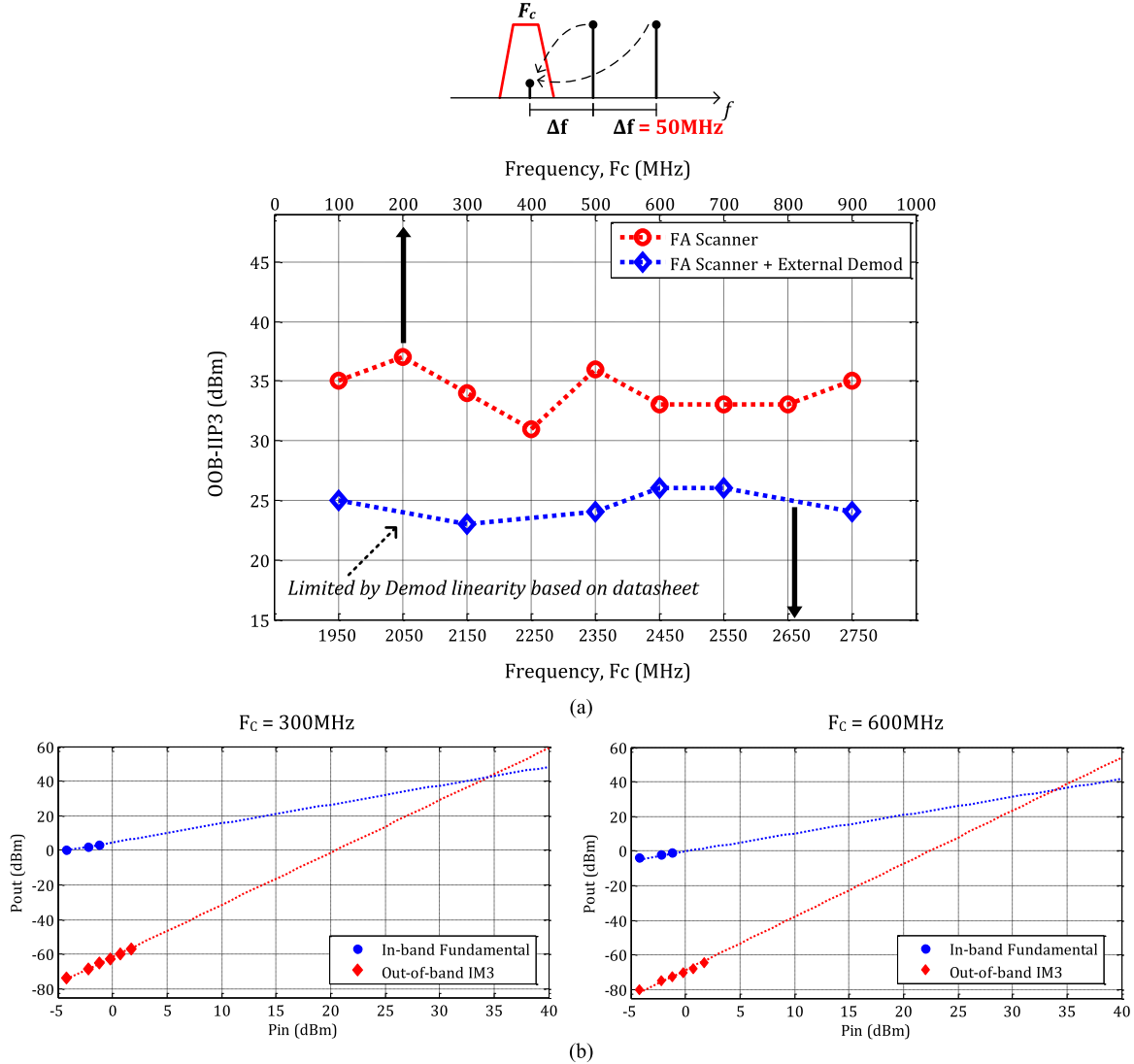


Fig. 22. (a) OOB-IIP3 versus center frequency of the FA Scanner with and without the external demodulator. (b) Pout versus Pin for two example filters.

coupled to scan a 1 GHz spectrum and 2) using an upfront external demodulator (LTC5585) to extend the input scanning range. When using the external demodulator, two separate FA IC's were used for the I and Q paths. Since the output of the filters is a sampled-and-held signal at rate F_S , any input signal frequency greater than $F_S/2$ (around the carrier frequency of the filter) gets attenuated and aliases back into the 0 to $F_S/2$ band. Hence, unlike conventional continuous-time systems, the filter responses are generated by providing tonal inputs and measuring the aliased signal acquired at baseband after sampling. For example, with $F_S = 10$ MHz, for any center frequency, an input at 101 MHz when passed through the LPTV RC circuit gets suppressed and aliases back to 1 MHz, whereas an input at 106 MHz would alias back to 4 MHz. Off-chip buffers are used to drive these filtered outputs.

On IC-startup, the RDAC is calibrated to a 9-b level and the measured values are used to generate the filter responses. Programmability in the capacitor bank helps account for any global changes in these measured resistance values. Fig. 19 shows the normalized measured frequency response as the

resistor sequence, and hence, the center frequency is varied to scan across the different frequency bins using the baseband setup. Similar responses were obtained with the demodulator setup as well. A representative measured filter response at 100 MHz is also shown, indicating an analog resolution bandwidth (RBW) of 10 MHz with an in-band ripple of $\sim 1.5\text{--}2$ dB and a sharp transition bandwidth of 20 MHz, making it an equivalent sixth-order BPF. Fig. 20 shows the worst case spurious images as the center frequency is varied. The measured stopband attenuation is close to what was expected based on circuit parasitics. The HR, however, is lower than predicted due to an unexpected on-board capacitance, C_P at the chip input in addition to the circuit parasitics. As shown in Section IV-A, this parasitic capacitance C_P also causes a first-order gain roll-off as the filter center frequency, F_C is swept across the 1 GHz span. Furthermore, as mentioned previously, the inherent filter *sinc* shape also causes a systematic gain variation of ~ 3 dB across the 1 GHz band. While the effect of the *sinc* shape is known at filter design time, C_P is readily estimated and both effects are corrected for digitally. Fig. 21

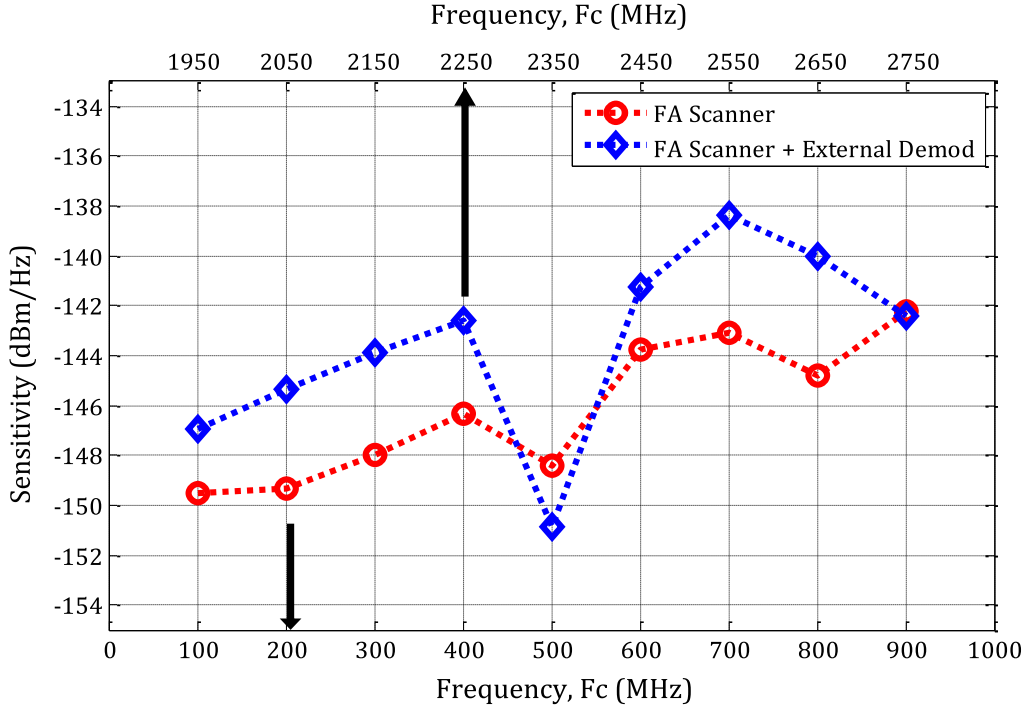


Fig. 23. Sensitivity versus center frequency of the FA Scanner with and without the external demodulator for 0 dB SNR.

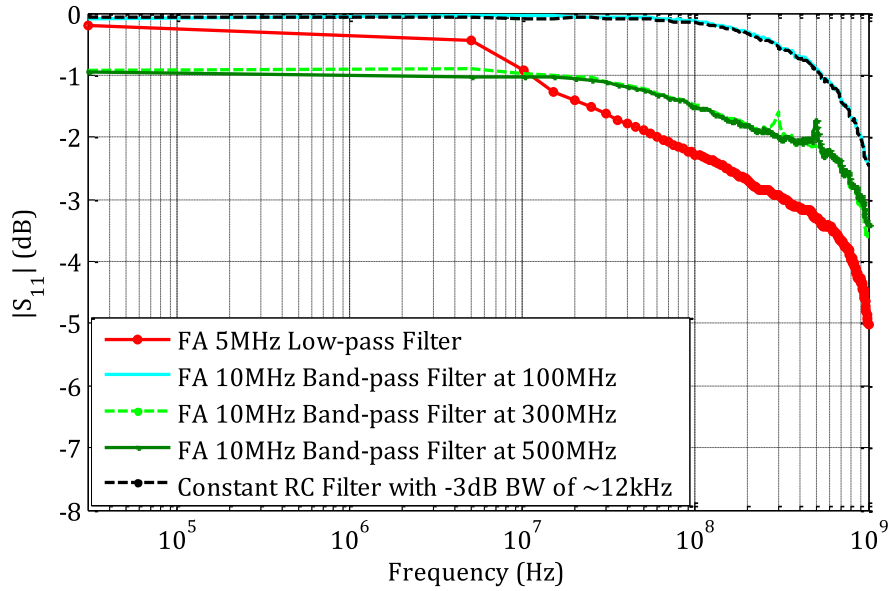


Fig. 24. Measured $|S_{11}|$ for the passive LPTV scanner.

shows the gain variation as the center frequency is varied. Note that the residual OOB signals (due to limited stopband attenuation and/or HR) can alias back in-band, leading to false detection. Future work on this scanner aims to address this issue.

Figs. 22 and 23 show the OOB IIP3 and sensitivity of the FA scanner, respectively, both by itself and with the external demodulator. The results with the demodulator are for the upper sideband with the demod LO set at 1850 MHz. Similar results were obtained for the lower sideband as well. The FA scanner is highly linear with an OOB IIP3 of $>+31$ dBm across the band. The P_{in} versus P_{out} curves for two example

FA filters are also shown in Fig. 22. The measured OOB IIP3 is at least $+21$ dB higher than any other comparable spectrum scanner prior art; Tohidian *et al.* [17] presents a very linear filter as well, however, it only performs low-pass filtering. In the presence of the external demodulator, the IIP3 worsens due to the limited linearity of the demod used. Based on the LTC5585 datasheet, the demod has a linearity of $\sim+25$ dBm in the measured frequency range. The measured sensitivity (assuming a 0 dB SNR) of the FA scanner by itself is better than -142 dBm/Hz and matches the expected value for the 32.5 pF capacitance used with the output sampling rate of 10 MHz. The upward trend in the scanner sensitivity as the

TABLE I
PERFORMANCE SUMMARY AND COMPARISON TO PRIOR ART

	This work	Goel [5]	Alink [6]	Ingels [7]-[8]	Yazicigil [3]
Technology	65nm	130nm	65nm	40nm	65nm
Architecture	Filtering by Aliasing	Dual Up/Down Conversion	Cross-Correlation	Digital and Analog Multi-band Sensing	Compressive Sensing
Circuit Implementation	Passive	Active	Active	Active	Active
Supply (V)	1.2(A), 1(D)	1.8	1.2	1.1	1.1
Frequency Span (GHz)	0 - 1	0.1 - 6	0.3 - 1	0.5 - 2.5	2.7 - 3.7
Power (mW)	< 8 ^a	227	36-61	33-99	81
OOB IIP3 (dBm)	> +31	+10	+5 ^b	-16	N/R
OOB IIP2 (dBm)	+70	+40	N/R	+53	N/R
Sensitivity (dBm/Hz)^c	< -142	-145	-158 ^d	N/R	-142 ^e
NF (dB)	26	N/R	10	7	N/R
SFDR in 1MHz RBW (dB)	75	63	69	61	N/R
Worst-case Spurious Image (dB)	-24	N/R	-27 ^f	N/R	N/R
Analog RBW (MHz)	10,20 ^g	0.4-11	20	0.2-20	10,20
Scan Time for 20MHz Analog RBW and 1GHz Span^h (us)	50	50 ⁱ	50	50	4.4 ^j
Spectrum Occupancy Constraints	None	None	None	None	Sparse (6%) ^j
Active Die Area (mm²)	1.68 ^k	14.43	0.15	5.2	1.96

^a Excluding output buffer, and ADC; ^b IB/OOB not specified; ^c specified for 0dB SNR; ^d -172dBm/Hz using cross-correlation with maximum sensing time; ^e Measured using 80 samples with a $P_D = 90\%$ and $P_{FA} < 15\%$; ^f Obtained from [18] which expands on [6]; ^g Measured BWs, others achievable using programmable resistor waveforms; ^h 1MHz digital RBW; ⁱ 20MHz analog RBW not supported; ^j For a maximum of 3, 20MHz bins in 1GHz span; ^k 0.5mm² area is occupied by the extra capacitance added for debug

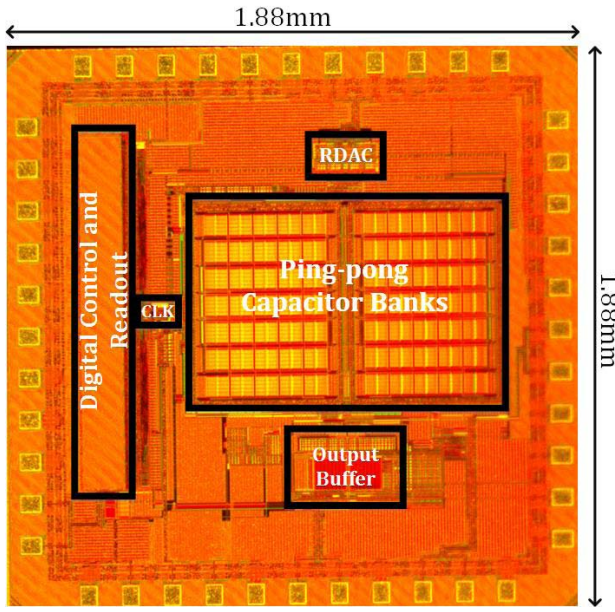


Fig. 25. Chip micrograph.

filter center frequency is increased is related to the gain plot in Fig. 21. Due to the passive structure, the filter loss directly translates to reduced sensitivity. Power consumption is weakly dependent on F_C with worst case observed for $F_C \sim F_{CLK}/2$: the switch drivers draw 2.1 mA from 1.2 V while the digital

and clock generation blocks draw 4 and 1.4 mA, respectively, from 1 V for a total power consumption of 8 mW. For a 1 MHz digital RBW (combined with a 20 MHz analog RBW), the scan time for a serial scan of the 1 GHz spectrum is 50 μ s. The S_{11} measurement for the scanner is shown in Fig. 24. It should be noted that at high frequencies the board capacitance C_P mentioned previously affects the S_{11} as well.

Table I summarizes the results for the FA scanner and compares it to other state-of-the-art designs. The presented work is a passive solution that provides the best linearity and lowest power compared to other designs. Although some solutions offer better sensitivity than this work, their spurious-free-dynamic range and power draw is significantly higher. Fig. 25 shows the chip micrograph. The active die area is 1.68 mm².

VI. CONCLUSION

This paper introduced a passive filter-based approach to spectrum scanning. The filters themselves use an LPTV resistor technique for creating sharp, programmable low-pass or band-pass filters based on the recently developed FA principle. The scanners developed were highly programmable and showed unprecedented performance in terms of linearity and power. Measured worst case harmonic image rejection, however, may be too high for some applications. Future work is expected to further improve the scanner's filter performance

including HR (especially by carefully studying the effect of circuit parasitics).

APPENDIX I LPTV RC EQUIVALENT LTI FILTER

Recall that $h(t, \tau)$ is the response of the circuit at time “ t ” for an impulse applied at time “ $t - \tau$.” With $x(t) = \delta(t - \tau)$, the initial voltage on the capacitor is related to the resistance value at that instance and given by $y_0 = 1/[R(t - \tau)C]$. This voltage will then decay through varying time-constants as the resistance changes from $R(t - \tau)$ to $R(t)$. Applying KCL at the capacitor node, $y_C(t)$, we have

$$\frac{y_C(t)}{R(t)} = -C \frac{d}{dt} y_C(t). \quad (12)$$

Solving the above differential equation and using the initial condition y_0 , we get

$$h(t, \tau) = \frac{1}{R(t - \tau)C} \exp\left(-\int_0^\tau \frac{du}{R(t-u)C}\right). \quad (13)$$

The equivalent LTI impulse response is simply $h_{eq}(\tau) = h(0, \tau) = h(T_S, \tau)$.

APPENDIX II NOISE IN A TIME-VARYING RC CIRCUIT

We show below that even with a time-varying resistance, the mean square noise voltage on the capacitor of the LPTV RC circuit is kT/C , and it is independent of when it is sampled. We start with the autocorrelation of the thermal noise input of the resistor, $E[x(t)x(t+v)] = 2kTR(t)\delta(v)$, where k is the Boltzman constant, T is the temperature in Kelvin and $R(t)$ is the resistance value at a given instance. Then for the output noise power, we have

$$\sigma_{y(t)}^2 = E[y(t)^2] = \int_0^\infty h^2(t, \tau) 2kTR(t-\tau)d\tau. \quad (14)$$

Replacing $h(t, \tau)$ in (14) with (13) from Appendix I, and substituting $u = \int_0^\tau (dv/(R(t-v)C))$, it follows that:

$$\sigma_{y(t)}^2 = \int_0^\infty 2KT \frac{1}{C} \exp(-2u) du = \frac{kT}{C}. \quad (15)$$

REFERENCES

- [1] M. Nekovee, “Cognitive radio access to TV white spaces: Spectrum opportunities, commercial applications and remaining technology challenges,” in *Proc. IEEE Symp. Frontiers Dyn. Spectr.*, Apr. 2010, pp. 1–10.
- [2] B. Murmann, *ADC Performance Survey 1997–2015*, accessed on 2016. [Online]. Available: <http://web.stanford.edu/~murmarr/adcsurvey.html>
- [3] R. T. Yazicigil, T. Haque, M. R. Whalen, J. Yuan, J. Wright, and P. R. Kinget, “A 2.7-to-3.7 GHz rapid interferer detector exploiting compressed sampling with a quadrature analog-to-information converter,” in *IEEE Int. Solid-State Circuits Conf. (ISSCC) Dig. Tech. Papers*, San Francisco, CA, USA, Feb. 2015, pp. 1–3.
- [4] M. Mishali, Y. C. Eldar, O. Dounaevsky, and E. Shoshan, “Xampling: Analog to digital at sub-Nyquist rates,” *IET Circuits, Devices Syst.*, vol. 5, no. 1, pp. 8–20, Jan. 2011.
- [5] A. Goel, B. Analui, and H. Hashemi, “A 130-nm CMOS 100-Hz-6-GHz reconfigurable vector signal analyzer and software-defined receiver,” *IEEE Trans. Microw. Theory Techn.*, vol. 60, no. 5, pp. 1375–1389, May 2012.

- [6] M. S. O. Alink, E. A. M. Klumperink, A. B. J. Kokkeler, Z. Ru, W. Cheng, and B. Nauta, “Using crosscorrelation to mitigate analog/RF impairments for integrated spectrum analyzers,” *IEEE Trans. Microw. Theory Techn.*, vol. 61, no. 3, pp. 1327–1337, Mar. 2013.
- [7] M. Ingels *et al.*, “A 5 mm² 40 nm LP CMOS 0.1-to-3 GHz multistandard transceiver,” in *IEEE Int. Solid-State Circuits Conf. Dig. Tech. Papers*, Feb. 2010, pp. 458–459.
- [8] S. Pollin *et al.*, “Digital and analog solution for low-power multi-band sensing,” in *Proc. IEEE Symp. Frontiers Dyn. Spectr.*, Apr. 2010, pp. 1–2.
- [9] D. Cabric, A. Tkachenko, and R. W. Brodersen, “Spectrum sensing measurements of pilot, energy, and collaborative detection,” in *Proc. IEEE Military Commun. Conf. (MILCOM)*, Oct. 2006, pp. 1–7.
- [10] N. Sinha, M. Rachid, and S. Pamarti, “An 8 mW, 1 GHz span, passive spectrum scanner with > +31 dBm out-of-band IIP3,” in *Proc. IEEE Radio Freq. Integr. Circuits Symp. (RFIC)*, May 2016, pp. 278–281.
- [11] M. Rachid, S. Pamarti, and B. Daneshrad, “Filtering by aliasing,” *IEEE Trans. Signal Process.*, vol. 61, no. 9, pp. 2319–2327, May 2013.
- [12] N. Sinha, M. Rachid, and S. Pamarti, “A sharp programmable passive filter based on filtering by aliasing,” in *Symp. VLSI Circuits Dig. Tech. Papers*, Jun. 2015, pp. 16–19.
- [13] S. Hameed, N. Sinha, M. Rachid, and S. Pamarti, “A programmable receiver front-end achieving >17dBm IIP3 at <1.25×BW frequency offset,” in *IEEE Int. Solid-State Circuits Conf. Dig. Tech. Papers (ISSCC)*, Jan./Feb. 2016, pp. 446–447.
- [14] S. Pavan and R. S. Rajan, “Inter-reciprocity in linear periodically timevarying networks with sampled outputs,” *IEEE Trans. Circuits Syst. II, Express Briefs*, vol. 61, no. 9, pp. 686–690, Sep. 2014.
- [15] M. Grant and S. Boyd. (Apr. 2011). *CVX: Matlab Software for Disciplined Convex Programming*, Version 1.21. [Online]. Available: cvxr.com/cvx
- [16] S. Wu, S. Boyd, and L. Vandenberghe. *FIR Filter Design Via Spectral Factorization and Convex Optimization*, accessed on 2012. [Online]. Available: <http://www.ee.ucla.edu/~vandenberghe/publications/magdes.pdf>
- [17] M. Tohidian, I. Madadi, and R. B. Staszewski, “Analysis and design of a high-order discrete-time passive IIR low-pass filter,” *IEEE J. Solid-State Circuits*, vol. 49, no. 11, pp. 2575–2587, Nov. 2014.
- [18] O. Alink and M. Stefan, “RF spectrum sensing in CMOS exploiting crosscorrelation,” Ph.D. thesis, Dept. Elect. Eng., Math. Comput. Sci., Univ. Twente, Enschede, Netherlands, 2013.



Neha Sinha (S’13) received the bachelor’s degree in applied science (Honors, Co-op) in electrical engineering from the University of Waterloo, ON, Canada, in 2010, and the M.S. degree from the University of California, Los Angeles, CA, USA, in 2012, where she is currently pursuing the Ph.D. degree in the integrated circuits and systems track.

From 2006 to 2009, she has done internships at Kapik Integration, Toronto, ON, Canada, Sun Microsystems, Santa Clara, CA, USA, and ON Semiconductor, Waterloo, ON, Canada. Her current research interests include mixed-signal circuit design and application of signal processing techniques for circuit enhancements.

Ms. Sinha was a recipient of the NSERC PGS-M during 2010–2011 and PGS-D during 2012–2015 scholarships from the Government of Canada.



Mansour Rachid (S’02) received the B.E. degree in computer and communications engineering from the American University of Beirut, Beirut, Lebanon, in 2006, and the M.S. and Ph.D. degrees in electrical engineering from the University of California, Los Angeles, CA, USA (UCLA), in 2009 and 2013, respectively, with an emphasis on wireless integrated circuits and systems.

In 2011, he was with Maxlinear, Inc., Carlsbad, CA, USA, where he developed digital correction algorithms for nonlinear receiver front-ends. In 2013, he was a Post-Doctoral Scholar with the Electrical Engineering Department, UCLA. He is currently a Principal Research and Development Engineer with Silvus Technologies, Inc., Los Angeles. His current research interests include multi-disciplinary adaptive signal processing algorithms and circuits with a main focus on distributed multi-antenna wireless networks and sensors.



Shanthi Pavan (SM'12) received the B.Tech. degree in electronics and communication engineering from IIT Madras, Chennai, India, in 1995, and the M.S. and Sc.D. degrees from Columbia University, New York, NY, USA, in 1997 and 1999, respectively.

From 1997 to 2000, he was with Texas Instruments, Warren, NJ, USA, where he was involved in high-speed analog filters and data converters. From 2000 to 2002, he was involved in microwave IC's for data communication at Big bear Networks, Sunnyvale, CA, USA. Since 2002, he has been with

IIT Madras, where he is currently a Professor of Electrical Engineering. His current research interests include high-speed analog circuit design and signal processing.

Dr. Pavan was a recipient of the IEEE Circuits and Systems Society Darlington Best Paper Award in 2009, the Shanti Swarup Bhatnagar Award in 2012, the Swarnajayanthi Fellowship in 2009 (from the Government of India), the Mid-career Research Excellence Award, the Young Faculty Recognition Award from IIT Madras (for excellence in teaching), the Technomenter Award from the India Semiconductor Association, and the Young Engineer Award from the Indian National Academy of Engineering (2006). He has authored *Understanding Delta-Sigma Data Converters* (second edition), with R. Schreier and G. Temes. He has served as the Editor-in-Chief of the IEEE TRANSACTIONS ON CIRCUITS AND SYSTEMS: PART I—REGULAR PAPERS, and on the editorial boards of both parts of the IEEE TRANSACTIONS ON CIRCUITS AND SYSTEMS. He has served on the technical program committee of the International Solid State Circuits Conference, and been a Distinguished Lecturer of the Solid-State Circuits Society. He is a fellow of the Indian National Academy of Engineering.



Sudhakar Pamarti (S'98–M'03) received the B.Tech. degree in electronics and electrical communication engineering from IIT, Kharagpur, India, in 1995, and the M.S. and the Ph.D. degrees in electrical engineering from the University of California, San Diego, CA, USA, in 1999 and 2003, respectively.

From 1995 to 1997, he was with Hughes Software Systems, New Delhi, India, where he was involved in the development of embedded software and firmware for a wireless-in-local-loop communication system.

From 2003 to 2005, he was with Rambus Inc., Sunnyvale, CA, USA, where he was involved with high-speed I/O circuits. He is a Professor of Electrical Engineering with the University of California, Los Angeles, CA, USA.

Dr. Pamarti was a recipient of the National Science Foundation's CAREER Award for developing digital signal conditioning techniques to improve analog, mixed-signal, and radio frequency integrated circuits. He currently serves on the Technical Program Committee of the IEEE Custom Integrated Circuits Conference and as an Associate Editor of the IEEE TRANSACTIONS ON CIRCUITS AND SYSTEMS: PART I—REGULAR PAPERS.